Supporting Information for

Bubble Nucleation and Growth on Microstructure Surface under Microgravity

Qiushi Zhang[1], Dongchuan Mo[1], Jiya Janowitz[2], Dan Ringle[2], David Mays[2], Andrew Diddle[2], Jason Rexroat[2], Eungkyu Lee[1,*], and Tengfei Luo[1,3,*]

1. Department of Aerospace and Mechanical Engineering, University of Notre Dame, IN, USA

2. Space Tango Inc., 611 Winchester Rd. Lexington, KY, USA

3. Department of Chemical and Biomolecular Engineering, University of Notre Dame, IN, USA

* Corresponding authors: eleest@khu.ac.kr; tluo@nd.edu.

SI1. Fabrication of Microstructured Cu Substrates.

As shown in the **Figure 1a** of main text, these microstructured Cu substrates were fabricated by the so-called hydrogen bubble template electrodeposition method.[1,2] The Cu substrates were prepared as cylinders with a diameter of ~35 mm and thickness of 0.5 mm before being cleaned with dilute sulfuric acid, hot dilute caustic solution, and deionized water.[3] A cleaned Cu substrate was then used as the cathode in the setup shown in **Figure 1a**. Another Cu plate was placed ~2 cm apart from the cathode substrate to act as the anode. The electrodeposition process was performed in a stationary solution in which the molarity of H_2SO_4 was kept at 0.8 M with the molarity of $CuSO_4$ ranging from 0.2 M to 1.0 M for different substrates (C1 to C4). A DC power supply (Maynuo 8852) was used for the deposition process, in which the Cu atoms in anode were dissolved into the solution and formed Cu^{2+} ions. These Cu^{2+} ions were driven by the electric field to move toward and finally be deposited onto the cathode Cu substrate. However, if the input current density is high enough, a hydrogen evolution reaction can occur simultaneously with the Cu^{2+} ions deposition process on the cathode to initiate the hydrogen bubble template electrodeposition (**Figure 1a**). These abundant hydrogen bubbles generated on the cathode can be used as the template to construct microporous structures on the cathode Cu substrate. By controlling the molarity of $CuSO_4$, we can control the porosities of the microporous structures on Cu substrates, i.e., the porosity increases as the molarity of $CuSO_4$ increases. The deposition process lasted for 60 s each with a current density of 1 $A \cdot cm^{-2}$. After the Cu substrates were rinsed with deionized water and dried, they were sintered in reducing atmosphere at 710 ºC for 30 mins to strengthen the microstructure.[4] **Figure 2b** shows the optical microscope images of the Cu substrates.

SI2. Finite element thermofluidic surface bubble nucleation transient simulations.

We employed COMSOL Multiphysics to simulate the transient temperature and flow profiles around the Cu substrate in the boiling system on ground or in space. The flow effect, thermal conduction and convection (ground model) in liquid are included in our simulations. The details of the model used in our simulations are shown in **Figure 3a**. There are several conditions that have been assumed in our simulations: (1) The liquid flow and heat transfer are both transient. Figures S1 and S2 show the flow velocity fields and temperature profiles of ground and space models at t = 3, 10 and 20 s, respectively. (2) In the liquid water, the flow is laminar (compressible with gravity on ground, compressible without gravity in space, see **Figure 3a** for the direction of gravity on ground), which satisfies the following momentum equation:

on ground,

$$\rho\frac{\partial\vec{u}}{\partial t}+\ \rho(\vec{u}\cdot\nabla)\vec{u}-\nabla\cdot\left(\ \mu\left(\overleftrightarrow{\nabla u}+\overleftrightarrow{\nabla u}^{\mathrm{T}}\right)-\ \frac{2}{3}\mu(\nabla\cdot\vec{u})\overleftrightarrow{I}-p\overleftrightarrow{I}\right)-\ \rho\vec{g}=0 \qquad \text{(s1)}$$

, and in space,

$$\rho\frac{\partial\vec{u}}{\partial t}+\ \rho(\vec{u}\cdot\nabla)\vec{u}-\nabla\cdot\left(\ \mu\left(\overleftrightarrow{\nabla u}+\overleftrightarrow{\nabla u}^{\mathrm{T}}\right)-\ \frac{2}{3}\mu(\nabla\cdot\vec{u})\overleftrightarrow{I}-p\overleftrightarrow{I}\right)=0 \qquad \text{(s2)}$$

and continuity equation:

$$\frac{\partial\rho}{\partial t}+\ \nabla\cdot(\rho\vec{u})=0 \qquad \text{(s3)}$$

where ρ is the density of water, μ is the dynamic viscosity of water, $\vec{u}$ is the velocity

vector, p is pressure, t is time, $\vec{g}$ is gravity constant, and $\overleftrightarrow{I}$ is a 3×3 identity matrix. (3) The SiO_2 cuvette and Cu substrate are considered as rigid solid materials. (4) The heat generation rate (Q) of Cu substrate is the only heat source, which supplies the heat to the liquid water with the following heat transfer equations:

In water,

$$\rho C_p \frac{\partial T}{\partial t} + \rho C_p \vec{u} \cdot \nabla T - k_w \nabla^2 T = Q \quad \text{(s4)}$$

where C_p is the heat capacity of water at constant pressure, T is the temperature, k_w is the thermal conductivity of water, Q is the heat generation rate by Cu substrate, and in the medium of SiO_2 or Cu,

$$-k_s \nabla T = q \quad \text{(s5)}$$

where k_s is the thermal conductivity of SiO_2 or Cu, and q is the heat flux coming through the liquid/solid interfaces. The boundary conditions used in our simulations are similar to those in ref. [5–7]. The heat generation rate is:

$$Q = \frac{P}{V_0} \quad \text{(s6)}$$

where P is the heating power and V_0 is the volume of the Cu substrate. To note, the heat generation rate of space models (C1 and C4 substrates) and ground model is the same, which is calibrated by letting the max. temperature on the substrate on ground being slightly higher than the nucleation temperature (422 K) at the end of simulation (**Figure**

3b).

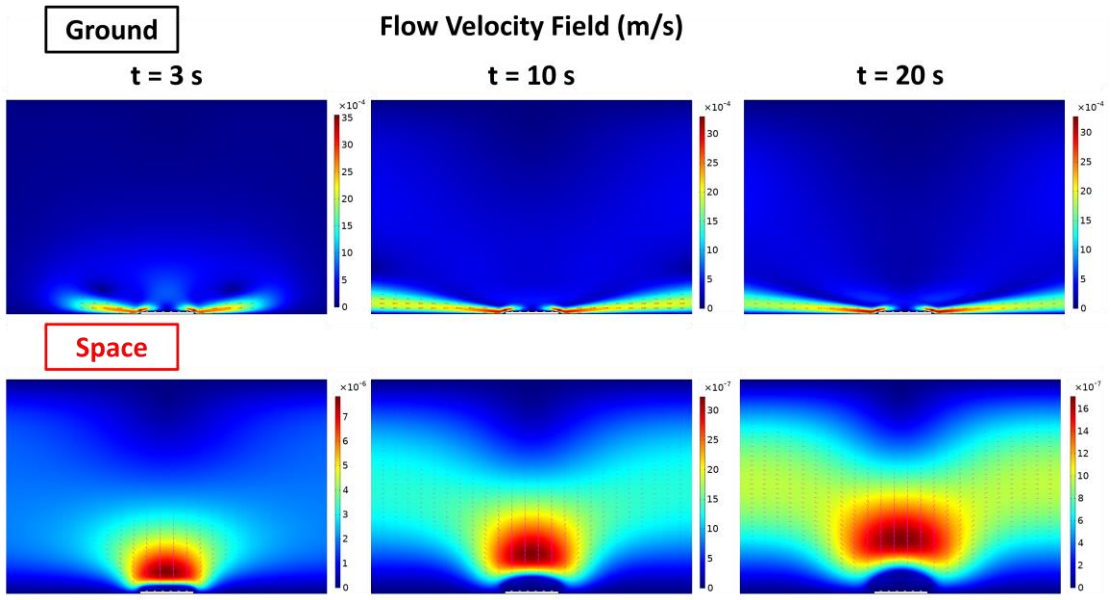

Figure S1. The flow velocity fields of ground (upper) and space (lower) models at t = 3, 10 and 20 s.

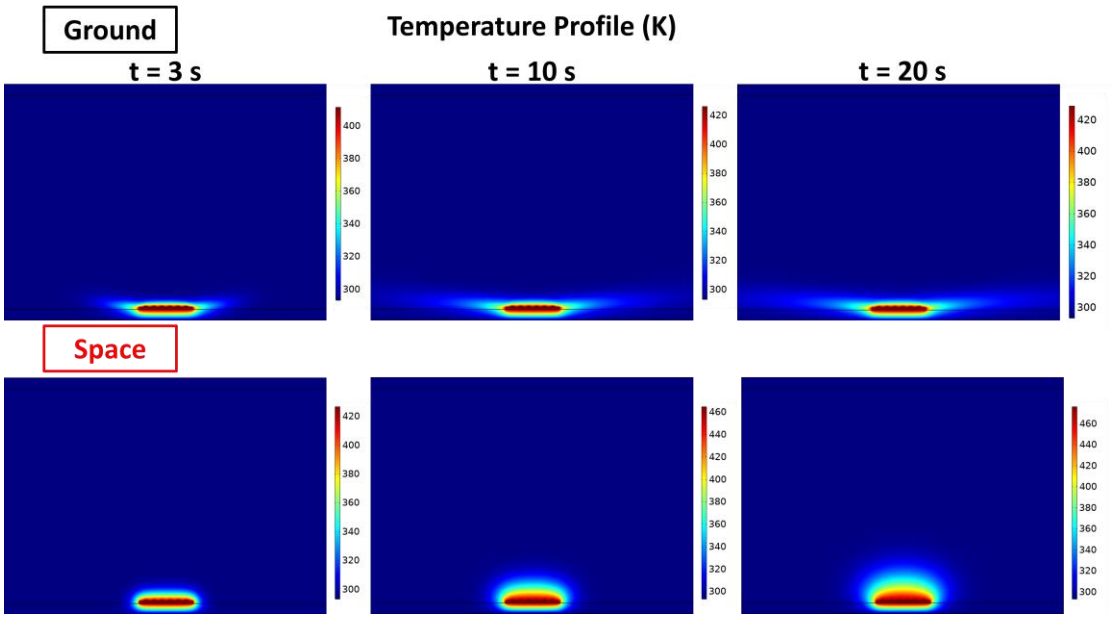

Figure S2. The temperature profiles of ground (upper) and space (lower) models at t = 3, 10 and 20 s.

As the experimental setup described in **Figure 1c** shows, the heat was provided by a Peltier (10 mm × 10 mm) affixed to the outside of the cuvette and conducted through the cuvette wall to the Cu substrate (20 mm × 20 mm) for surface bubble nucleation to occur. However, in order to simply our simulation models, we instead set the Cu substrate as the heat source of the boiling system in this work. To check if the heating effect of our model can represent the real experimental setup, we repeated the simulations of bubble nucleation on ground and in space while using a more realistic model, i.e., with another layer of Cu (half of the size of the Cu substrate) as the external heater to heat up the Cu substrate in the boiling system (Figure S3a). As we can see in the simulated temperature profile (Figure S3a), the heat from the external heater is conducted through the cuvette wall and mostly concentrated on the Cu substrate without any significant leakage into the cuvette wall that not covered by the Cu substrate. This is because the heat conductivity of Cu is ~2 orders of magnitude larger than SiO_2. As a result, this indicates that by setting the Cu substrate as the heater of the boiling system can achieve similar heating effect as the experimental system, which is also evidenced by the similar flow field and max. surface temperature plots shown in Figures S3b and c, respectively (compared to **Figures 3b and c**).

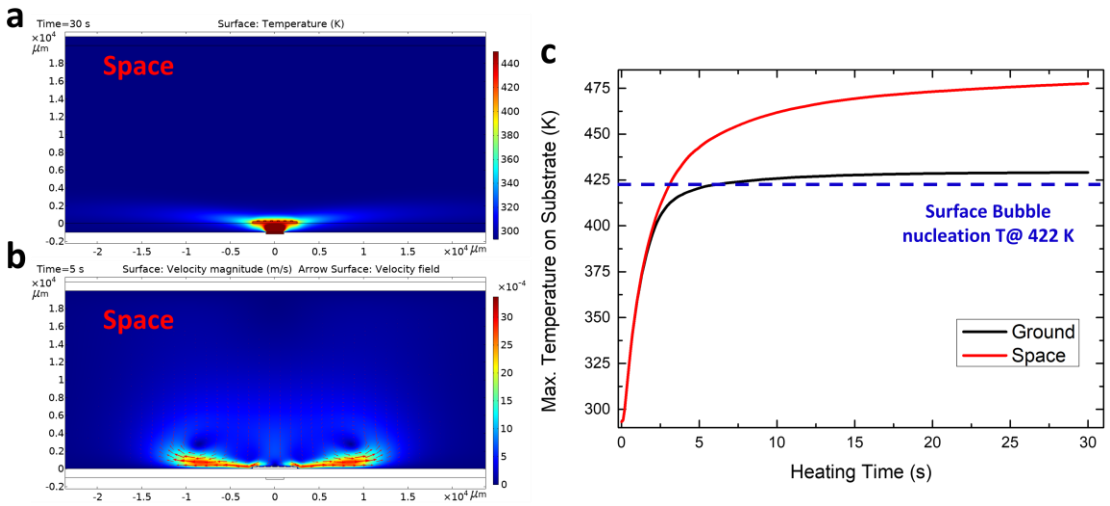

Figure S3. The simulated temperature profile at t = 30 s (a) and flow velocity field at t = 5 s (b) of space model using the model with external heater (compared to **Figures 3b and c**). (c) The simulated max. temperatures on substrate as a function of heating time on ground (black) and in space (red) using the model with external heater. The bubble nucleation temperature at ~422 K is indicated by a blue dash line.

SI3. Finite element thermofluidic surface bubble growth steady-state simulations.

The model and assumptions of bubble growth simulations are similar to those in the bubble nucleation simulations described in section SI2, while the liquid flow and heat transfer are at steady state. In liquid water, the momentum equation is:

on ground,

$$\rho(\vec{u}\cdot\nabla)\vec{u} - \nabla\cdot(\mu(\overleftrightarrow{\nabla u} + \overleftrightarrow{\nabla u}^{\mathrm{T}}) - p\overleftrightarrow{I}) - \rho\vec{g} = 0 \quad \text{(s7)}$$

, and in space,

$$\rho(\vec{u}\cdot\nabla)\vec{u} - \nabla\cdot(\mu(\overleftrightarrow{\nabla u} + \overleftrightarrow{\nabla u}^{\mathrm{T}}) - p\overleftrightarrow{I}) = 0 \quad \text{(s8)}$$

, and continuity equation is:

$$\rho(\nabla\cdot\vec{u}) = 0 \quad \text{(s9)}$$

where the definitions of variables are the same as those in equations (s1), (s2) and (s3), respectively. The heat transfer equation in water is:

$$\rho C_p\vec{u}\cdot\nabla T - k_w\nabla^2 T = Q \quad \text{(s10)}$$

where the definitions of variables are the same as those in equation (s4). The heat generation rate also follows the same equation as equation (s6). An air bubble with a radius of 3 mm was added on top of the Cu substrate (**Figure 5d**). The gas medium

inside the surface bubble, quartz walls and Cu substrate were considered as non-fluidic rigid materials, which have the same heat transfer equation as equation (s5). The interface of the bubble (gas/water boundary) has a slip boundary condition with the Marangoni effect as:

$$\left[\mu\left(\overleftrightarrow{\nabla u}+\overleftrightarrow{\nabla u}^{\mathrm{T}}\right)-\left(p+\frac{2}{3}\mu(\nabla\cdot\vec{u})\right)\overleftrightarrow{I}\right]\hat{n}=\gamma\nabla_t T \qquad \text{(s11)}$$

where $\hat{n}$ is the normal outward vector to the surface of the bubble, γ is the temperature derivative of the water/gas surface tension, and ∇_t is the gradient of the tangent vector to the surface of the bubble.

References:

1. Shin, H.-C. & Liu, M. Copper Foam Structures with Highly Porous Nanostructured Walls. *Chem. Mater.* **16**, 5460–5464 (2004).
2. Wang, Y.-Q., Mo, D.-C. & Lyu, S. Enhanced Pool Boiling Heat Transfer on Mono and Multi-Layer Micro-Nano Bi-Porous Copper Surfaces. in (American Society of Mechanical Engineers Digital Collection, 2016). doi:10.1115/MNHMT2016-6544.
3. Wang, Y.-Q., Luo, J.-L., Heng, Y., Mo, D.-C. & Lyu, S.-S. Wettability modification to further enhance the pool boiling performance of the micro nano bi-porous copper surface structure. *International Journal of Heat and Mass Transfer* **119**, 333–342 (2018).
4. Xu, P., Li, Q. & Xuan, Y. Enhanced boiling heat transfer on composite porous surface. *International Journal of Heat and Mass Transfer* **80**, 107–114 (2015).
5. Zhang, Q. *et al.* Light-Guided Surface Plasmonic Bubble Movement via Contact Line De-Pinning by In-Situ Deposited Plasmonic Nanoparticle Heating. *ACS Appl. Mater. Interfaces* **11**, 48525–48532 (2019).
6. Zhang, Q. *et al.* Surface Bubble Growth in Plasmonic Nanoparticle Suspension. *ACS Appl. Mater. Interfaces* **12**, 26680–26687 (2020).
7. Zhang, Q., Li, R., Lee, E. & Luo, T. Optically Driven Gold Nanoparticles Seed Surface Bubble Nucleation in Plasmonic Suspension. *Nano Lett.* **21**, 5485–5492 (2021).